Plasma Physics and Controlled Fusion, Vol. 31, No. 6, pp. 921 to 939, 1989
Printed in Great Britain.

0741-3335/89 $3.00+ .00

EFFECT OF ANTENNA PHASING AND WALL CONDITIONING ON ICRH IN TEXTOR

A. MESSIAEN,* J.-M. BEUKEN, L. DE KEYSER, T. DELVIGNE, P. DESCAMPS,†
F. DURODIE, M. GAIGNEAUX, M. JADOUL, R. KOCH, D. LEBEAU, J. ONGENA,
X. M. SHEN,‡ P. E. VANDENPLAS, R. VAN NIEUWENHOVE, G. VAN OOST,
G. VAN WASSENHOVE and R. R. WEYNANTS*

Laboratoire de Physique des Plasmas–Laboratorium voor Plasmafysica, Association "Euratom-Etat belge"–Associatie "Euratom-Belgische staat", Ecole Royale Militaire–Koninklijke Militaire School, B-1040 Brussels, Belgium

T. BANNO,§ G. BERTSCHINGER, P. BOGEN, Y. CAO,‡ H. CONRADS, K.-H. DIPPEL,
H. G. ESSER, K.-H. FINKEN, G. FUCHS, B. GIESEN, E. GRAFFMANN, H. HARTWIG,
E. HINTZ, F. HOENEN, K. HOETHKER, B. KARDON,‖ L. KOENEN, M. KORTEN,
Y. T. LIE, V. PHILIPPS,¶ A. POSPIESZCZYK, D. RUSBUELDT, U. SAMM, J. SCHLUETER,
B. SCHWEER, H. SOLTWISCH, F. WAELBROECK, G. WAIDMANN, P. WIENHOLD,
J. WINTER and G. H. WOLF

Institut für Plasmaphysik, Kernforschungsanlage Jülich, GmbH, Association "Euratom-KFA", D-5170 Jülich, F.R.G.

and

R. W. CONN, W. J. CORBETT and D. M. GOEBEL

Institute of Plasma and Fusion Research and Department of Mechanical, Aerospace and Nuclear Engineering, University of California, Los Angeles, CA 90024, U.S.A.

(*Received* 12 *July* 1988; *and in revised form* 19 *December* 1988)

Abstract—Four new low field side antennae grouped in pairs have been installed on TEXTOR. It is found that the interaction with the wall (density rise, impurity generation) is significantly reduced when operating each pair out of phase (π) as opposed to in phase (0). The beneficial effect in the π configuration is obtained without drop in plasma loading. This experimental property is shown, from theory, to be explained by the judicious choice of the geometrical configuration.

A further improvement in the wall interaction is made possible by an appropriate choice of wall conditioning (wall carbonization with liner at 400°C or, above all, boronization). As a result record low values of P_{rad}/P_{total} were achieved during ICRH. The large reduction in wall interaction during ICRH allows routine long pulse (> 1 s) ICRH operation at the maximum power level available ($\cong$ 2.5 MW).

1. INTRODUCTION

THE ICRH system hitherto used on TEXTOR has been described in various papers (see e.g. VAN OOST *et al.*, 1987) and its performance discussed therein. Two independent heating lines are each fed by one 1.5 MW generator. Before 1987 each line

* Research director at the NFSR, Belgium.
† EEC grantee of the Institut für Plasmaphysik, KFA, Jülich, F.R.G.
‡ Institute of Plasma Physics, Academia Sinica, Hefei, P. R. China.
§ Department of Applied Physics, University of Tokyo, Japan.
‖ Central Research Instutute for Physics, Budapest, Hungary.
¶ Institut für Chemie 1, KFA Jülich, F.R.G.

was connected at the low field side (LFS) to a $\lambda/4$ half-turn antenna (called OLD in this paper). The two antennae were placed in the same poloidal plane so that they completely surrounded the plasma and provided mostly a high field side (HFS) excitation. This antenna configuration resulted in mode conversion in a (H)–D plasma as the main heating scenario. At sufficiently low concentration of the H minority, so-called minority or $\omega = 2\,\omega_{CD}$ heating was also possible (MESSIAEN *et al.*, 1986*a*; WOLF *et al.*, 1986; KOCH *et al.*, 1987). It was shown (WEYNANTS *et al.*, 1985; MESSIAEN *et al.*, 1986*a*; WOLF *et al.*, 1986; VANDENPLAS *et al.*, 1987) that an essential prerequisite for the successful application of ICRH in TEXTOR was a proper wall conditioning of the machine by wall carbonization consisting of coating with a dense hydrogenated carbon film (Winter, 1987). Prior to the application of this procedure (WAIDMANN *et al.*, 1984), all the r.f. heated discharges switched at rather low power levels into strong detachment (not yet recognized as such at that time) (WEYNANTS *et al.*, 1987, 1988*a*; VANDENPLAS, 1987) rapidly evolving to disruption. Stationary low impurity conditions were obtained with carbonization (MESSIAEN *et al.*, 1986*a*): the sum of the central metallic impurity concentrations relative to the plasma density n_e, measured by X-ray spectroscopy, ranged from 10^{-5} to 10^{-4} in the OH discharge and increased by a constant amount $\cong 6 \times 10^{-5}$ during the application of 1 MW of r.f. power. The main contribution to Z_{eff} was due to light impurities, C and O, and no significant increase in Z_{eff} was observed during ICRH. On the other hand, a rise of D flux was noted during ICRH resulting in an increase of the line average density.

In 1987 a new antenna system, compatible with the ALT II toroidal pump limiter requirements, was installed on TEXTOR. It consisted of four identical LFS antennae which were grouped in two pairs (of electrical length $\lambda/7$), each one radially movable with respect to the liner, situated at diametrically opposite toroidal positions in the Tokamak. In Fig. 1a a picture is shown of one pair of antennae whereas the detailed mechanical layout is given in Fig. 1b. The temperature of the liner and of the antennae can be externally adjusted. Each antenna pair can be fed in phase or out of phase by one 1.5 MW generator. These phasing configurations are respectively named 0 and π in the paper. The motivation for using the π configuration was to launch waves with larger $k_\parallel$ having better absorptivity and therefore interacting less with the wall. The beneficial effect of the π phasing in achieving lower impurity conditions has already been observed in various experiments (see e.g. for TFR : Equipe TFR, 1985; for JFT-2M : TAMAI *et al.*, 1986; for JET : BURES *et al.*, 1988*a* and for TFTR : WILSON *et al.*, 1988). On JIPP T-llu (ANDO *et al.*, 1988), on the other hand, an improvement of the heating efficiency was observed with no significant effect on the impurities.

The practical problem encountered in most experiments with π phasing (see e.g. BURES *et al.*, 1988) is that the loading resistance is usually lower than with 0 phasing and that the antenna power capability, limited by its voltage standoff value, is consequently lower. The TEXTOR antenna has been designed in order to have roughly the same loading for the two phase configurations. This point is discussed in the next section together with the experimental results. The favourable effect of the π phasing and of the choice of the wall conditioning on the plasma wall interaction are discussed in Section 3. The best methods are either wall carbonization with the liner brought to a temperature of 400°C during Tokamak discharges, or wall boronization. This is obtained by a wall coating process with a film consisting of a mixture of roughly 50% boron and 50% carbon (WINTER *et al.*, 1988). After such appropriate

wall conditioning the contribution of the metallic impurities to the total radiation can be neglected (central radiation less than 10 mW cm^{-3} in Ohmic discharges and less than 60 mW cm^{-3} with 2.6 MW of ICRH and boronized wall); only this case is considered in the present paper.

2. COUPLING PROPERTIES OF A NEW ANTENNA PAIR

2.1. *Coupling theory*

The voltage V_A to be applied at the input of an antenna of the pair, neglecting Ohmic losses, in order to launch an active power P_A ($2P_A$ per pair) at a frequency $\omega/2\pi$ is given by (WEYNANTS *et al.*, 1980; MESSIAEN and WEYNANTS, 1982)

$$|V_A| = (2P_A/G_A)^{1/2}, \tag{1a}$$

where

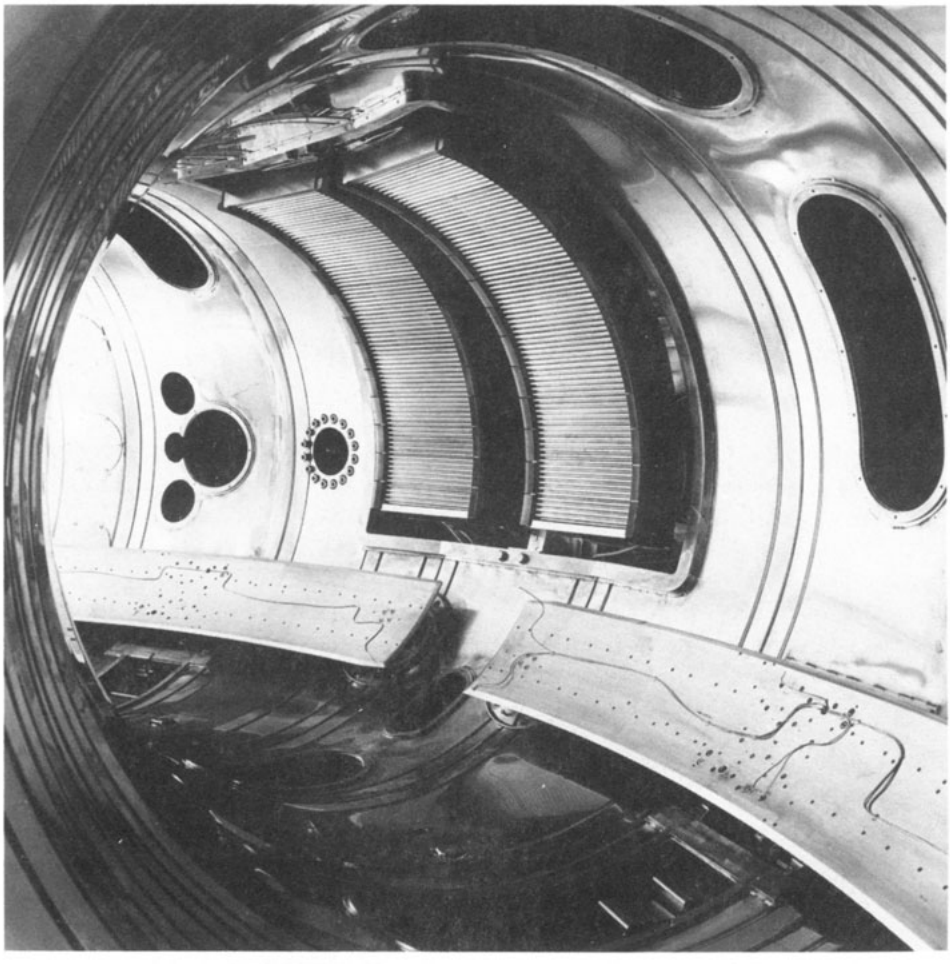

FIG. 1(a).—View of one pair of new movable ICRH antennae installed in the TEXTOR liner. Parts of the toroidal belt limiter ALT II are seen underneath.

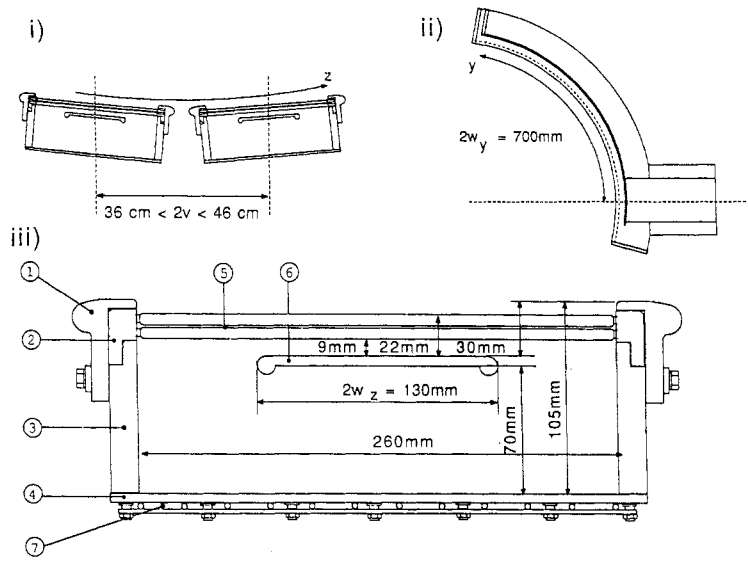

FIG. 1(b).—Toroidal (i) and poloidal (ii) sections of the antenna. In the toroidal section of one antenna of the pair (iii), the following are identified: (1) carbon side limiters, (2) exchangeable Faraday shield element holders, (3) side walls, (4) return conductor, (5) Faraday shield, (6) central conductor, (7) antenna baking system.

$$G_A = \frac{R}{(\omega L)^2 l} f_1(\beta l) \tag{1b}$$

is the antenna input conductance, $l = 2w_y$ is the antenna length (along the poloidal y direction) and $1 < f_1 < 1.23$ for $0 < l/\lambda < 1/4$. We have also $\beta = 2\pi/\lambda \cong \omega\sqrt{LC}$ where R, L and C are respectively the specific loading resistance, self inductance and capacitance of the strip line antenna (WEYNANTS *et al.*, 1980). C is not influenced by the plasma and L, which is mostly determined by the near field, decreases only slightly when the plasma density in front of the antenna rises (see Fig. 4b). The behaviour of G_A then depends mostly on the plasma loading R.

The 3-D coupling theory allowing the computation of R has been discussed in detail in various references (BHATNAGAR *et al.*, 1982*a*, MESSIAEN *et al.*, 1982; KOCH *et al.*, 1986*b*). Taking into account the periodicity $2\pi R_A$ along the toroidal z direction and the periodicity $2\pi r_A$ along the poloidal y direction, one obtains the specific loading resistance R from a double Fourier integral of the form:

$$R\int_0^l I^2\,\mathrm{d}y = \frac{\omega\mu_0}{(2\pi)^2 R_A r_A}\int\int\sum_m\sum_n \delta\left(k_z - \frac{m}{R_A}\right)\delta\left(k_y - \frac{n}{r_A}\right) g\,|\mathcal{J}|^2\,\mathrm{d}k_z\,\mathrm{d}k_y \tag{2}$$

where $I = I_0 \cos \beta y$ is the r.f. current flowing on the strip line antenna. The function $g\ (k_z, k_y)$ is the plasma coupling function which depends on the radial dimensions of the antenna system and, sensitively, on the plasma profile in front of the antenna (see the inset of Fig. 2a). For all cases considered here, we assume single pass absorption (as in the usual experimental conditions no strong eigenmodes are observed, see Section 2.2), obtained in the model by taking a constant density $n = n_0$ for

$-b > x > -\infty$. The function $\mathcal{J}(k_z, k_y)$ is the antenna excitation function which depends on the transverse dimensions of the antenna system (width $2\ w_z$ of each antenna, distance $2\ v$ between the centers of the antennae of the pair: see Fig. 1b) and also on its length $2w_y$ and the propagation factor β along it. The functions g and $\mathcal{J}$ correspond respectively to the functions g'_3 defined in equation (4) of BHATNAGAR

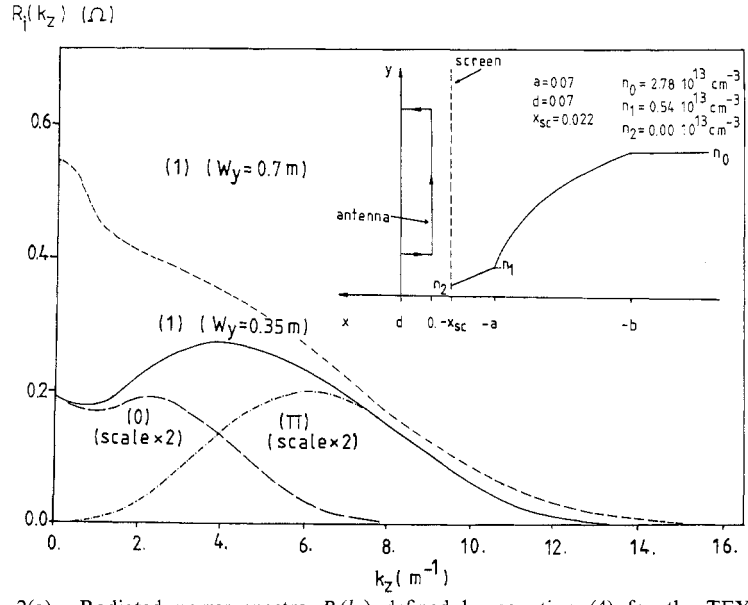

FIG. 2(a).—Radiated power spectra $R_i(k_z)$ defined by equation (4) for the TEXTOR antennae and the density profile indicated in the insert. Curves (1) are for a single antenna, curves (0) and (π) respectively for the 0 and π phasing configurations of the pair. The curve (1) in dotted line shows the effect of increasing the antenna length of a single antenna ($\omega/2\pi = 29$ MHz, $\beta = 1.17\ m^{-1}$, distances expressed in meters).

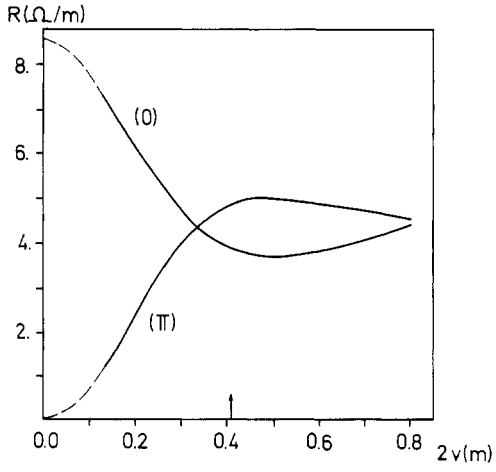

FIG. 2(b).—Influence of the distance $2v$ between the two antennae of a pair on the value of the loading resistance R for the radial density profile of Fig. 2(a). The dotted line corresponds to the region where the two antennae overlap. The arrow shows the actual value of $2v$ in TEXTOR.

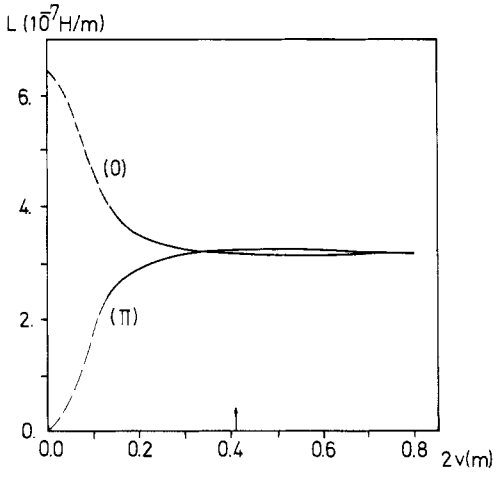

FIG. 2(c).—Same as (b) but for L as a function of $2v$.

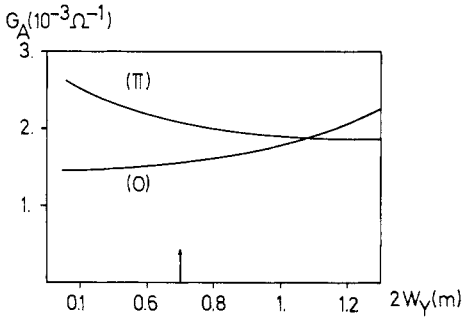

FIG. 2(d).—Influence of the antenna length $2w_y$ on the input antenna conductances for the radial density profile of Fig. 2(a) and the actual value of $2v$ in TEXTOR. The arrow indicates the actual value of $2w_y$.

et al. (1982*a*) and $\mathcal{J}_L$ defined in equation (5a) of the same reference. We use the following subscripts to characterize the different antenna configurations which are discussed: 1 when only one antenna of the pair is fed, 0 when the two antennae are fed in phase or π when the two antennae are fed out of phase. For these three cases we have the following dependence of $\mathcal{J}$ on w_z and v (WEYNANTS *et al.*, 1980; MESSIAEN *et al.*, 1984)

$$\begin{vmatrix} \mathcal{J}_1 \\ \mathcal{J}_0 \\ \mathcal{J}_\pi \end{vmatrix} \propto \frac{\sin k_z w_z}{k_z w_z} \begin{vmatrix} 1 \\ \sqrt{2}\cos k_z v \\ \sqrt{2}\sin k_z v \end{vmatrix}. \tag{3}$$

The k_z spectrum of the radiated power is expressed by

$$R_i(k_z) = \frac{\omega\mu_0}{(2\pi)^2 r_A} \frac{\int \sum_n \delta\left(k_y - \frac{n}{r_A}\right) g |\mathcal{J}_i|^2 \, \mathrm{d}k_y}{\int_0^l I^2 \, \mathrm{d}y}; \quad i = 1, 0, \pi \tag{4}$$

such that the corresponding specific loading resistance R_i is given, from equation (2), by

$$R_i = \frac{1}{R_A}\int \sum_m \delta\left(k_z - \frac{m}{R_A}\right) R_i(k_z)\,\mathrm{d}k_z.$$

Typical examples of $R_i(k_z)$ are shown in Figs. 2a and 3a. Their k_z dependence can be understood on the basis of three features:

(i) the interference inherent in equation (3);

(ii) the decrease of g for increasing $|k_z|$ due to larger evanescence in the plasma edge;

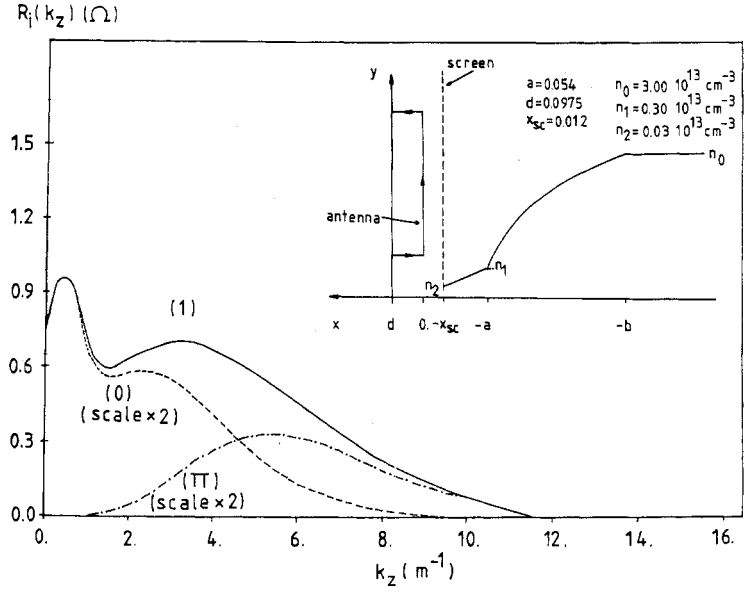

FIG. 3(a).—As Fig. 2(a) but for the A_1 antennae of JET ($\omega/2\pi$ = 33 MHz, β = 2.0 m^{-1}).

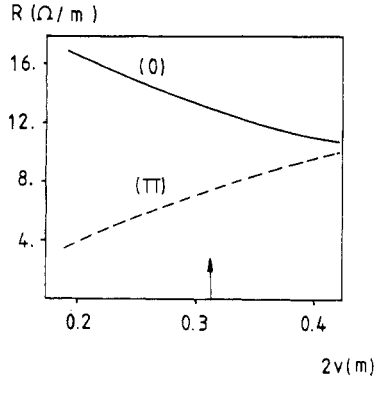

FIG. 3(b).—As Fig. 2(b) but for the JET case of Fig. 3(a).

(iii) a decrease of excitation at low k_z due to the finite length w_y as can be seen in Fig. 2a by comparing $R_1(k_z)$ for two values of w_y.

In our model we assume a vacuum layer to exist everywhere between the plasma and the wall: a low $|k_z|$ contribution to the loading can then also come from the excitation of coaxial modes (MESSIAEN *et al.*, 1982). These coaxial modes do not, however, exist for realistic plasma density values of the boundary layer ($d < x < -x_{sc}$) existing in most Tokamaks (MESSIAEN *et al.*, 1986*b*) and can be removed following a prescription given by DESCAMPS (1988). For the TEXTOR cases considered here all coaxial mode are below cut-off and their contributions are anyway negligible. The effect of the image currents on the antenna side limiters [which can be taken into account (BHATNAGAR *et al.*, 1982*b*)] is here disregarded.

To obtain equal loading with 0 or π phasing the following rules of thumb can be derived:

(a) A sufficiently large distance $2v$ between the two antennae of the pair should be provided such that g has not decreased too much with respect to g ($|k_z| = 0$) when $|k_z|$ equals $\pi/(2v)$, i.e. near the first maximum of $\sin k_z v$. The distance v on the other hand cannot be too large because each antenna would then act independently and the benefit of the k_z-spectrum shaping would be lost. A choice of the optimal value of v has been made for the TEXTOR antenna pair and the resulting spectra $R_i(k_z)$ are shown in Fig. 2a for the typical plasma density profile shown in the inset. Note that equation (3) implies that

$$2R_1 = R_0 + R_\pi, \tag{5}$$

an expression which is valid for both $R_i(k_z)$ from equation (4) and R from equation (2). The evolution as a function of v of the specific loading resistances R_π and R_0 is given in Fig. 2b. For completeness we also included in the calculation the results for $v = 0$ where the two antennae of the pair are coincident and for which $R_0 = 2R$, and $R_\pi = 0$. Depending on the value of v, either R_0 or R_π can be the larger of the two. However, as the voltage characteristics of the antenna pair depend on $G_A \propto R/L^2$, we have also shown, in Fig. 2c, the corresponding evolution of the antenna specific self-inductances for the two phase configurations. It is observed that as v increases, L_0 and L_π become rapidly equal [note that the relations $2L_1 = L_0 + L_\pi$, similar to (5), also hold]. The arrow indicates the actual value of v in TEXTOR. Note that SOELL and NOTERDAEME (1985) have mentioned the beneficial influence of large values of v in maximizing the power absorption in the plasma with π phasing.

The detailed behaviour of Fig. 2a also depends on the plasma profile and the influence of changes in the parameters n_1, n_0 and x_{sc} is discussed in Section 2.3.

(b) A relatively short antenna length ($2w_y = \lambda/7$) is preferable to a longer one ($2w_y = \lambda/4$). As discussed in connection with Fig. 2a, shortening the antenna length preferentially affects the low $|k_z|$ thus influencing R_0 much more than R_π. Roughly speaking, R_1 and R_0 scale like w_y whereas R_π is independent of w_y. Since L and β are not significantly modified as long as w_y does not become too small, equation (1b) then yields, when $2w_y \leqslant \lambda/4$, $G_{A,1}$ and $G_{A,0}$ values which are independent of w_y whereas $G_{A,\pi}$ varies approximately like $1/w_y$. This behaviour is shown in Fig. 2d where $G_{A,0}$ and $G_{A,\pi}$ are given as a function of w_y, the other parameters being those of Fig. 2a. However, it must be noted that a decrease of w_y goes along with an increase of antenna

susceptibility which has to be cancelled by an external susceptibility to avoid the VSWR increase in the transmission line feeding the antenna.

For comparison's sake the k_z spectra of R_1, R_0 and R_π corresponding to the A_1 antenna pair of JET (in the so-called "dipole" configuration; see geometry in BHATNAGAR *et al.*, 1986) are also shown in Fig. 3a together with the density profile assumed and the radial antenna geometry. The contribution of the coaxial modes has been removed. The distance v, is clearly too small to obtain $R_\pi \cong R_0$ and the coupling is lower in the case of the π phasing. Figure 3b shows that, for the same radial parameters, the antenna loading would become equal in the 0 and π configurations for a value of v nearly equal to that chosen for TEXTOR. Mechanical constraints however limit the choice of v. The relation between the specific loading resistance R computed here and the loading resistance as defined in JET, namely $R_c = Z_{0,f}/s$ where $Z_{0,f}$ and s are respectively the characteristic impedance and the VSWR in the coaxial feeder to the antenna, can be easily derived ($s = (1+|\Gamma|)/(1-|\Gamma|)$, $\Gamma = (1-Z_{0,f}Y_A)/(1+Z_{0,f}Y_A)$ where $Y_A = G_A + iB_A$ and B_A is the antenna input susceptibility; only if $B_A = 0$ do we have a simple relation $R_c = G_A Z_{0,f}^2$). The ratio of $R_{c,0}/R_{c,\pi}$, for the experimental distance $2v = 0.315$ m, is 1.8, a value which is in the range of the experimental observations (BURES *et al.*, 1988*a*).

2.2. *Experimental coupling results*

Large amplitude eigenmodes have only been observed in conditions of low plasma absorptivity (H concentration $\ll 1\%$) with the 0 phasing. With π phasing, large amplitude eigenmodes have never been seen; this is due to the difference in the radiated $k_\parallel$ spectrum which leads to a shape of R_π versus density which is less sensitive to the toroidal eigenmodes (KOCH *et al.*, 1988*b*; DESCAMPS *et al.*, 1989) and to a larger damping. An example of the fluctuations seen on R in the normal operating conditions' r.f. pulses is shown in Fig. 7 for the 0 and π configurations.

For a given geometry, the specific loading resistance is mostly determined by the plasma density profile in front of the antenna and, experimentally, R exhibits a linear increase when plotted versus the electron plasma density near the edge (at $r = 40$ cm). An approximate independence of R with respect to configuration (0 or π) for the same antenna–plasma distance and plasma edge characteristics is experimentally observed as shown on Fig. 4a. The measurements have been made for 60 kW $< P_A <$ 1.5 MW. A corresponding data set for the OLD antenna, which has a lower loading due to its geometry (KOCH *et al.*, 1986*a*) is also shown (200 kW $< P_A <$ 600 kW). The slight experimental decrease of L when the plasma loading rises and its independence of the choice of 0 or π configuration is shown in Fig. 4b. The value of the antenna input conductance G_A is given by $G_A/R \cong 1.3 \times 10^{-3}\ \Omega^{-2}$ m for each OLD antenna and by $G_A/R \cong 7 \times 10^{-4}\ \Omega^{-2}$ m for each antenna of the new pair. Using equation (1), one deduces that the following input antenna voltages $|V_A|$ are needed to radiate a power $P_{RF} = P_A - P_{losses} = 1$ MW (using the mean plasma loading resistance of Fig. 4a): (i) with the OLD $\lambda/4$ antenna: 36 kV for $R = 1.35\ \Omega$/m (including 0.15 Ω/m of Ohmic losses); (ii) with the new antenna pair: 19 kV for $R = 4.4\ \Omega$/m (including 0.4 Ω/m of Ohmic losses).

2.3. *Comparison of theoretical loading with experiments*

In Fig. 5a are displayed in solid lines the theoretical curves of $R_{0,\pi}$ versus n_e ($r = 40$ cm) computed for a plasma density profile of the general form shown in the insert of

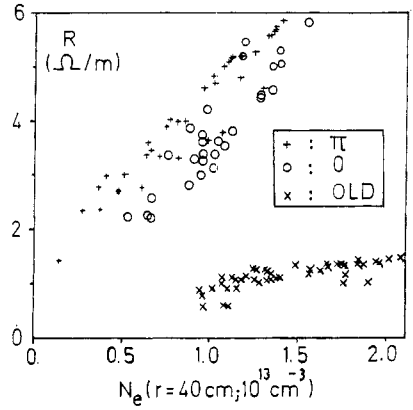

FIG. 4(a).—Experimental values of the specific loading resistance R, taking out the Ohmic losses, versus the edge density $n_e(r = 40$ cm) for the 0 and π phasing configurations of the new antennae and for the OLD antenna. [$I_p = 350$ kA, B_t 2T, D–(H) plasma, $\omega/2\pi = 29$ MHz for the new antennae and 28.6 MHz for the OLD one].

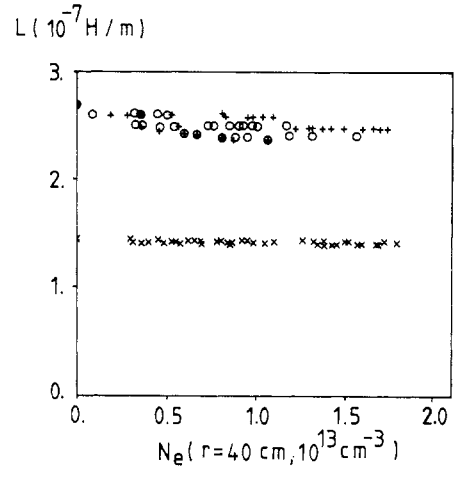

FIG. 4(b).—Corresponding evolution of the specific inductance L versus n_e ($r = 40$ cm).

Fig. 2a. The density profile $n = n_0[1-(r/(b-a))^\alpha]$ between n_0 and n_1 is fitted to the experimental density profile by imposing $n = n_e(r = 40$ cm) at 10 cm in front of the central conductor and by equating $n_0\,\alpha/\alpha+1$ with the central chord density $\bar{n}_{eo}$ ($r = 0$ corresponds to $x = -b = -50$ cm). A linear decrease of the density is assumed between $n = n_1$ at a distance $x = 7$ cm in front of the central conductor to $n = n_2 = 0$ at $x = x_{sc} = 2.2$ cm (outer part of the electrostatic screen). The corresponding theoretical curve for the OLD antenna parameters is also shown on the figure.

Whereas the theoretical curve R_π for the π phasing follows the experimental rise of R as a function of $n_e(r = 40$ cm), the curve R_0 increases with a lower slope. The difference in behaviour between R_0 and R_π occurs because the increase of density influences mostly the large $|k_z|$ part of the $g(k_z)$ spectrum in equation (2). The discrepancy of the theoretical R_0 evolution and the experimental one could be due to

the planar geometry approximation of the model or to the plasma profile chosen in front of the antenna.

The exact shape of the plasma profile in front of the antenna is not known. Edge plasma profiles are measured by laser ablation (POSPIESZCZYK *et al.*, 1988), thermal Li-beam spectroscopy (LIE *et al.*, 1984; POSPIESZCZYK *et al.*, 1988), and a fast scanning probe (GOEBEL *et al.*, 1988). Only this last diagnostic and one of the Li beams have a small connection length linking them to the center of the bottom part of one antenna pair (resp. 90 and 180 cm). Typical results of these diagnostics, shown in Fig. 5b and Fig. 5c, indicate a radial edge density profile perturbation during ICRH. However such an effect is, within the error bar, not seen by the laser ablation diagnostic (connection length of ~ 6 m to an antenna pair).

A rough modelling of the plasma shape modification in front of the antenna is

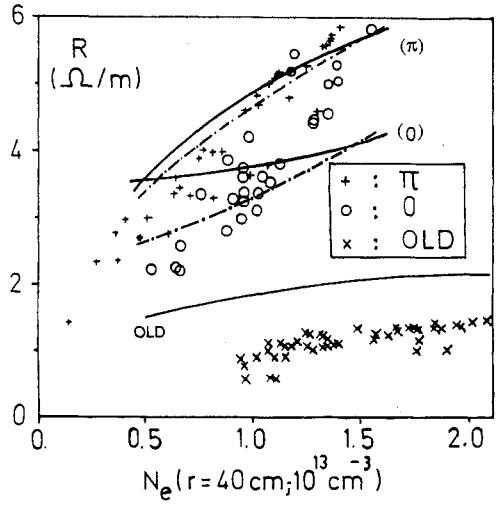

FIG. 5(a).—Experimental values of R (symbols) compared to 3-D code predictions for 0, π and OLD antenna cases (solid lines). The dotted lines are computed for a variable density profile in the vicinity of the antenna (defined in Section 2.3).

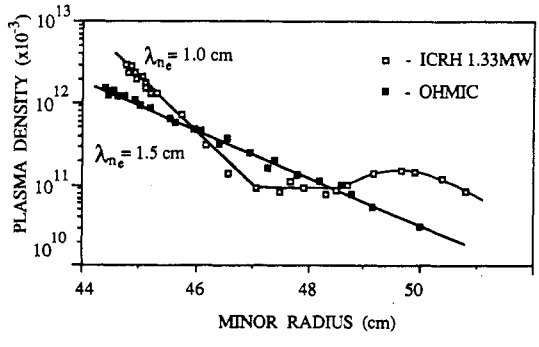

FIG. 5(b).—Density profile measured in OH and during ICRH by a fast scanning Langmuir probe. The main limiter (ALT-II) is at 44 cm, the antenna limiters at 46 cm and the outer edge of the electrostatic screen at 46.8 cm in this case. (Ohmic #31804, ICRH #31823).

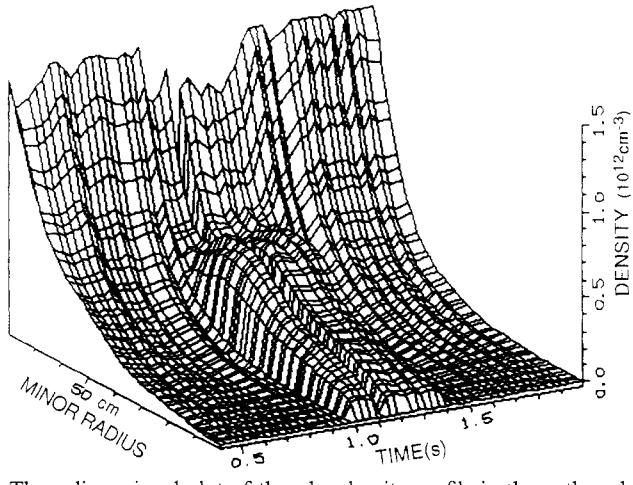

FIG. 5(c).—Three-dimensional plot of the edge density profile in the outboard side of the equatorial plane, as a function of time, obtained by thermal Li beam spectroscopy (#34427; $P_{RF} = 1.3$ MW from $t = 1.0$ up to 1.4 s; antenna limiter at 47 cm; ALT-II at 46 cm).

obtained by moving the position of x_{sc} away from the outer part of the electrostatic screen. We assume that x_{sc} increases from 2.2 cm to 6 cm when n_e ($r = 40$ cm) decreases from 1.5 to 0.5×10^{13} cm^{-3}. The corresponding R_π and R_0 curves are indicated by dotted lines in Fig. 5a. A large influence of a density depletion in front of the antenna is seen on R_0 because such a change of plasma profile affects mostly $g(k_z)$ for low values of $|k_z|$. A better modelling of the density profile modification in front of the antenna would require a precise knowledge of its dependence on n_{e0}, $P_{r.f.}$ and the phasing.

The fact that the experimental values of R, measured at low power (< 20 W, see KOCH *et al.*, 1988*a*), are in better agreement with the theoretical curve for the OLD case, might also indicate a profile modification at high power in front of the OLD antenna.

3. WALL INTERACTION

3.1. *Effect of antenna phasing*

The interaction between the plasma and the wall (liner and limiters) is significantly altered by switching from 0 to π antenna phasing for a given Tokamak wall condition. Figure 6 shows the dependence on the r.f. power coupled to the plasma, $P_{r.f.}$, of a number of relevant signals observed without density feedback control: the r.f. induced rise in line density $\Delta\bar{n}_e$, the increments in brilliance of a C_V and an O_{VI} spectroscopic line (ΔB_{CV} and ΔB_{OVI} respectively) and the global bolometric radiation increase ΔP_{rad}. The data pertain to a base OH plasma with $2.0 < \bar{n}_{e0}(10^{13}\,\text{cm}^{-3}) < 2.5$ with carbonized wall and a wall temperature T_L of 400°C. The data are selected from a series of shots where the two pairs of antennae are launching sequentially an r.f. pulse in the same plasma, one pair in the 0 configuration and the other in π (see Fig. 7).

The oxygen radiation is signifiantly lower with π phasing whereas the carbon radiation shows an opposite, yet much weaker tendency. As a result the total radiated

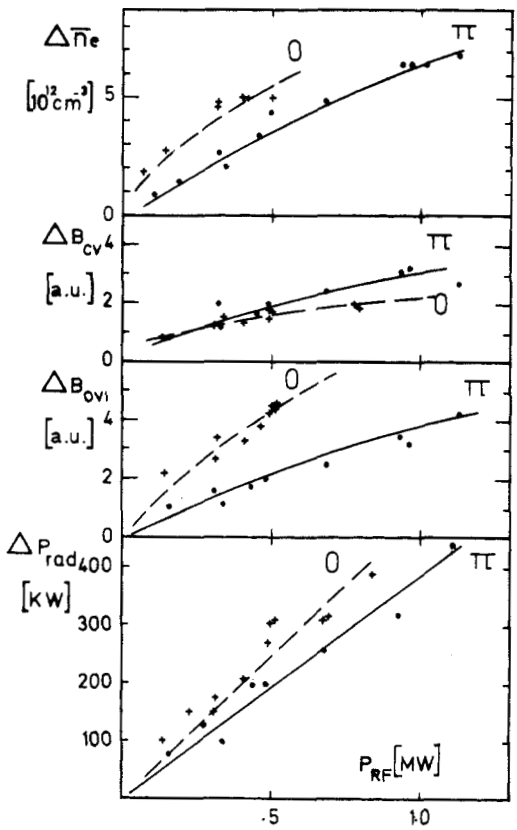

FIG. 6.—Increases of density, impurity line brilliance and total radiated power due to ICRH for 0 and π phasing (carbonized wall, $T_L = 400°C$).

power fraction γ and the incremental radiated power fraction γ_{inc} are lower for π phasing. The parameters γ and γ_{inc} are defined by the relations:

$$\gamma = \frac{P_{rad}}{P_{tot}}; \quad \gamma_{inc} = \left.\frac{(P_{rad} - P_{rad,OH})}{P_{tot} - P_{OH})}\right|_{same\ \bar{n}_{e0}}, \tag{6}$$

where P_{rad} is the total radiated power, $P_{rad,OH}$ and P_{OH} are respectively the radiated power and the OH power for an OH discharge with the same density and plasma current as for ICRH and for the same machine conditions; $P_{tot} = P_{r.f.} + P'_{OH}$ where P'_{OH} is the reduced ohmic power with ICRH. Due to the linear increase of ΔP_{rad} with $P_{r.f.}$ (as seen on Fig. 6) the value of γ_{inc} is roughly independent of $P_{r.f.}$ and is reduced from 0.5 with the 0 phasing to 0.4 with the π phasing in the conditions of Fig. 6.

The density increase $\Delta\bar{n}_e$ due to ICRH scales roughly as

$$\Delta\bar{n}_e = C\frac{P_{r.f.}^{0.8}}{\bar{n}_{e0}^{0.7}}, \tag{7}$$

as long as $\bar{n}_{e0} + \Delta\bar{n}_e$ remains sufficiently below the density limit, and has almost no I_p

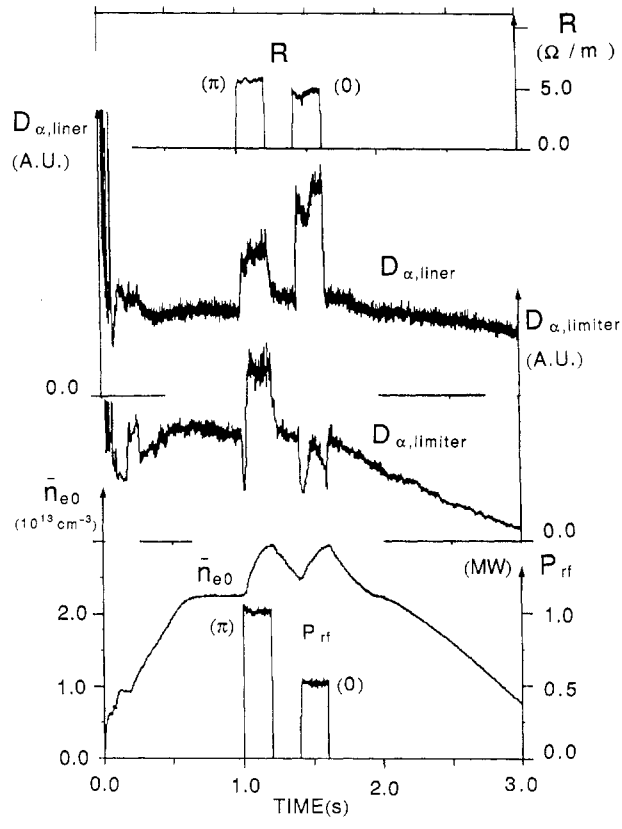

FIG. 7.—Evolution versus time of $P_{r.f.}$, $\bar{n}_{e0}$, D_α (limiter) and D_α (liner). The first r.f. pulse is with π phasing, the second r.f. pulse is with 0 phasing. The behaviour of the specific loading resistances is also shown. (Carbonized wall, $T_i = 400°C$, #31662.)

dependence. The values of C, for 0 and π phasing, are compared in Table 1 for a carbonized wall at 400°C.

The different impact on recycling of the 0 and π phase configurations is illustrated in Fig. 7 where the D_α emission at the liner and at the poloidal limiter is displayed versus time, together with $\bar{n}_{e0}$ for a shot during which one r.f. pulse of 1 MW is launched with the π phasing configuration followed by one pulse of 0.6 MW with 0 phasing. The reduction of limiter interaction together with the increase of interaction with the liner observed for the 0 phasing is typical of plasma detaching (WEYNANTS *et al.*, 1987, 1988*a*; SAMM and WEYNANTS, 1989) occurring here already at 600 kW. With the π phasing no sign of detachment is observed. This observation explains also the difference between the carbon and the oxygen radiation. Indeed, in TEXTOR the main source of carbon is the limiter whereas the oxygen mainly comes from the liner. The reduction of the deuterium flux incident on the limiter, in the zero phasing configuration, therefore leads to a relative reduction of carbon. On the other hand the increased interaction with the wall results in more oxygen in the discharge.

The decrease of the interaction with the wall can be correlated with the larger bulk

TABLE 1. PROPORTIONALITY FACTOR C OF THE ICRH-INDUCED DENSITY INCREASE IN TEXTOR FOR 0 AND π ANTENNA CONFIGURATIONS AND DIFFERENT MACHINE CONDITIONS. $\Delta\bar{n}_e = C P_{RF}^{0.8}\bar{n}_{e0}^{-0.7}$ WHERE $P_{r.f.}$ IS THE R.F. POWER EFFECTIVELY COUPLED (MW), $\bar{n}_{e0}$ IS THE PRE-R.F. DENSITY (10^{13} cm^{-3}) AND $\Delta\bar{n}_e$ IS THE R.F. INDUCED DENSITY RISE (10^{13} cm^{-3})

C	Machine Condition	Antenna configuration
2.9	Carbonization;T_L:150°C	O
1.65	Carbonization;T_L:400°C	O
1.1	Carbonization;T_L:400°C	π
0.55	Boronisation;T_L:150°C	π

absorption which is theoretically expected for the more optimized spectrum of the π phasing (BEUKEN *et al.*, 1988). Note that the amplitude of the observed toroidal eigenmodes is much lower with the π phasing, as discussed in Section 2.2, also pointing to a better single pass absorption for this case.

3.2. *Effect of wall conditioning*

The plasma–wall interaction during ICRH can furthermore be reduced by an appropriate choice of the wall conditions.

(i) In Table 1 the effect of the wall condition on the density increase $\Delta\bar{n}_e$ induced by ICRH [equation (7)] is shown for different wall conditions and antenna phasing. It appears that a factor 5 in reduction of $\Delta\bar{n}_e$ has been realized between the initial (0 phasing, carbonized wall at $T_L = 150$°C) and final boronized wall condition with π antenna phasing.

(ii) The values of γ, γ_{inc} and $\gamma_{OH} = P_{rad,OH}/P_{OH}$ which, for the same values of I_p, B_t and $\bar{n}_{e0}$ and the same machine conditions, are linked by the relation

$$\gamma = \gamma_{OH} P_{OH}/P_{tot} + \gamma_{inc}(1 - P_{OH}/P_{tot}), \tag{8}$$

are strongly dependent on this machine condition. This is shown on Fig. 8 where, for the two best conditions of Table 1 for ICRH operation, the values of γ_{OH} and γ_{inc} are displayed as a function of $\bar{n}_{e0}$ ($I_p = 0.35$ MA, $B_t = 2$T, D–(H) plasma, $N_H/N_D < 10\%$). The values of γ_{inc} have been obtained from shots with P_{tot} ranging from 0.8 to 2.5 MW.

The lower values of γ_{OH} and γ_{inc} for a given $\bar{n}_{e0}$ in the case of boronized wall is striking. Whereas γ_{OH} increases with $\bar{n}_{e0}$, γ_{inc} is roughly independent of $\bar{n}_{e0}$ and remains always lower than the fraction of radiated power γ_{OH} in a pure OH discharge. The fractions of radiated power can attain record low values during ICRH pulses for a boronized wall as seen e.g. in the example of Fig. 9. This is confirmed by the measurement of the heat load on the limiters which increases in accordance with the observed γ behaviour. The low metal concentration already found before (MESSIAEN *et al.*, 1986) is confirmed by the bolometric radial profile which remains hollow and steady during long (>1 s) ICRH pulses, showing no sign of metal pollution. For the highest power level the part of the radiation coming from the center of the plasma (<half

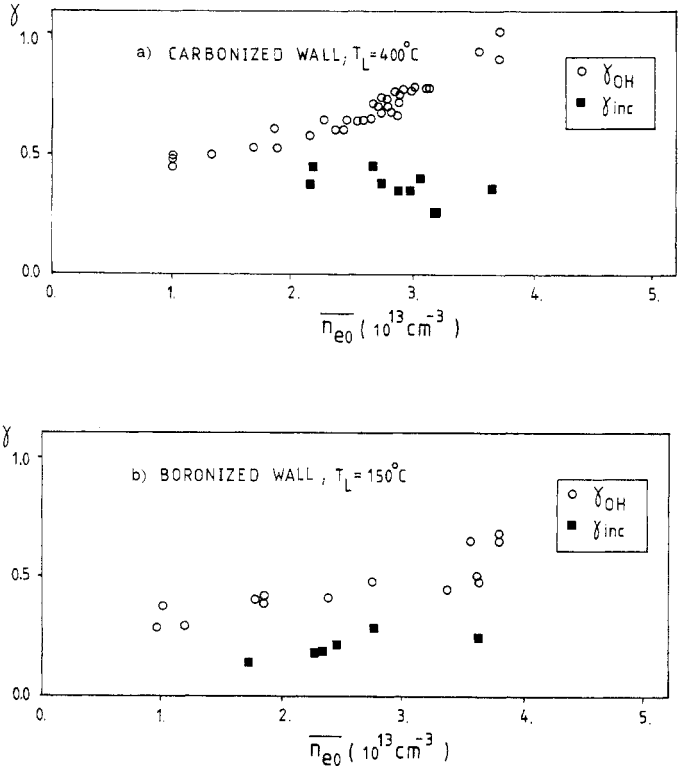

FIG. 8.—The evolution of the Ohmic (γ_{OH}) and incremental (γ_{inc}) radiated power fractions versus $\bar{n}_{e0}$: (a) in the case of carbonized wall and $T_L = 400°C$; (b) in the case of boronized wall and $T_L = 150°C$.

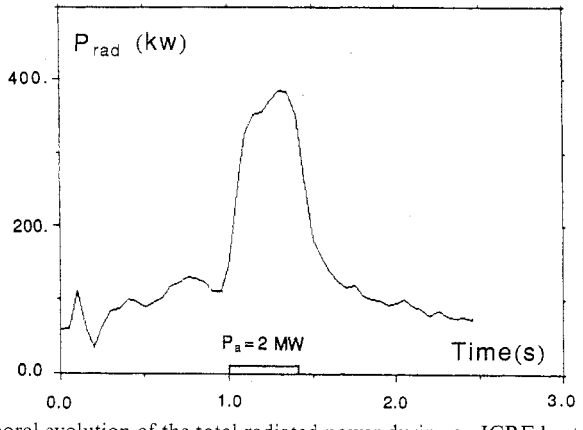

FIG. 9.—Temporal evolution of the total radiated power during an ICRF heated discharge. During the OH phase at $t = 0.9$ s, $\gamma = \gamma_{OH} = 0.35$ and $P_{tot} = P_{OH} = 0.34$ MW ($\bar{n}_{e0} = 1.0 \times 10^{13}$ cm^{-3}) whereas during ICRH at $t = 1.2$ s, $\gamma = 0.18$, $\gamma_{inc} = 0.15$ and $P_{tot} = 2.1$ MW ($\bar{n}_{e0} = 1.7 \times 10^{13}$ cm^{-3}). Case of boronized wall at $T_L = 150°C$ (#32144).

radius) remains as low as 6% of P_{tot} with boronization (see for details: WEYNANTS *et al.*, 1988*b*).

(iii) Due to the much easier density control achieved with a boronized wall it is possible to raise the r.f. power near the maximum available value (3 MW on matched load). This can be done not only at high density without exceeding the density limit but also at densities as low as $\bar{n}_{e0} = 2.2 \times 10^{13}$ cm^{-3}. Feedback control of the density is used to counteract any density change during r.f. An example of such a condition is shown in Fig. 10. For this shot $\gamma_{OH} = 0.43$ and during ICRH $\gamma = 0.20$ and $\gamma_{inc} = 0.17$. During ICRH the heat load on the poloidal limiter measured by infrared ther-

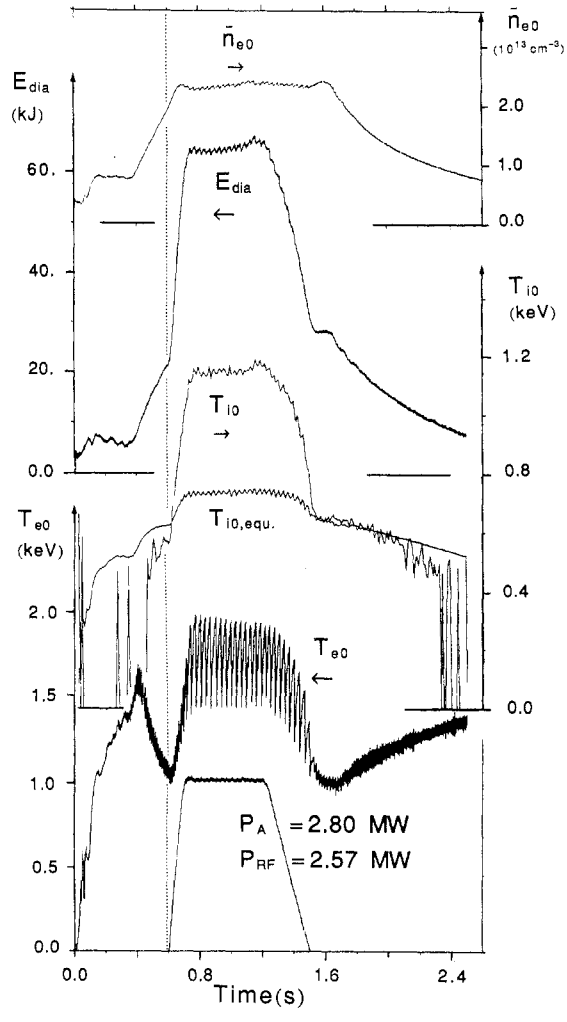

FIG. 10.—Diamagnetic energy E_{dia}, central chord density $\bar{n}_{e0}$, central electron temperature T_{e0} (from ECE), ion temperature T_{i0} (from neutron yield) and $T_{i0,equ}$ (computed from equipartition) together with the ICRH pulse ($P_A = P_{r.f.} + P_{losses}$) versus time for boronized wall conditions at $T_L = 150°C$ [$I_p = 0.35$ MA, $B_t = 2$T, D–(H), #32179]. The dotted line at $t = 0.6$ *s* indicates the beginning of the r.f. pulse.

mography (SAMM, 1983), parallel to the toroidal magnetic field is ~ 6.5 kW cm^{-2} ($P_{tot} = 2.8$ MW) whereas in OH discharges at the same density and machine condition it reaches 600 W cm^{-2} ($P_{OH} = 300$ kW). The evolution of the central values of the electron temperatures T_{e0} (from ECE), the ion temperatures T_{i0} (from the neutron yield), $T_{i0,equ}$ computed from T_{e0} assuming equipartition, and the behaviour of the diamagnetic energy are displayed.

The mechanisms leading to the improved situation resulting from the wall condition are discussed in WAELBROECK *et al.* (1988*a*, 1988*b*). The beneficial effect of a new carbonization or boronization lasts for several weeks of Tokamak operation.

In the optimum case, a doubling of both T_{e0} and T_{i0} is obtained with $P_{r.f.} = 2.5$ MW at $\bar{n}_{e0} = 2.3 \times 10^{13}$ cm^{-3}. Notwithstanding the change from HFS to LFS antennae, the heating efficiencies and the confinement properties are in line with the previously published results for the OLD antenna configuration. They are roughly independent of the phasing configuration or of the different wall conditions used. We obtain heating efficiencies $\eta_{e,i} = \bar{n}_{e0}\Delta T_{e,i}/P_{r.f.}$ somewhat below 1 keV $\times 10^{13}$ cm^{-3} MW^{-1} for the electrons and the ions and an incremental confinement time τ_{inc} (ms) $\cong 37 I_p$ (MA). In addition, however, an energetic hydrogen tail is observed due to the predominantly hydrogen minority heating scenario used with the present antennae (BEUKEN *et al.*, 1988; WEYNANTS *et al.*, 1988*b*).

4. CONCLUSIONS

It has been shown that in TEXTOR the interaction with the wall is reduced by the use of antenna pairs with π phasing without loss of the power capability of the antenna system. The design considerations enabling to achieve this have been discussed and the interest of choosing antenna pairs with sufficiently large separation and not too long electrical length has been demonstrated. The interaction with the wall and more particularly the ICRH-induced density rise have been further strongly reduced by operating either with carbonized wall at high temperature (400°C) or, even better, with boronized wall. The ratio γ of radiated power to total input power is lower during ICRH than during the pure OH discharge phase, decreasing to very low values with boronized wall (typically 0.2); for all conditions the metal pollution can be kept very low.

The achieved reduction of plasma-wall interaction allows routine long pulse (> 1 s) ICRH operation on TEXTOR near the maximum power available (2–2.8 MW).

Acknowledgement—We thank Dr D. FAULCONER for his careful perusal of the manuscript.

REFERENCES

ANDO R. *et al.* (1988) *Nucl. Fusion* **28**, 577.
BEUKEN J. M. *et al.* (1988) Proc. 15th Eur. Conf. on Controlled Fusion and Plasma Heating, Dubrovnik, Vol. 12B, Part II, p. 774.
BHATNAGAR V. P. *et al.* (1982*a*) *Nucl. Fusion* **22**, 280.
BHATNAGAR V. P. *et al.* (1982*b*) Proc. 3rd Joint Varenna-Grenoble Int. Symposium, Grenoble, Vol. 1, p. 325.
BHATNAGAR V. P. *et al.* (1986) Proc. 13th Eur. Conf. on Controlled Fusion and Plasma Heating, Schliersee, Vol. 10C, Part II, p. 77. See also JET-IR(86)07, p. 61.
BURES M. *et al.* (1988*a*) *Plasma Phys. Contr. Fusion* **30**, 149.

BURES M. *et al.* (1988*b*) Paper presented at the ICRF/Edge Physics Workshop, Boulder. See also KOCH R. *et al.*, Laboratory for Plasma Physics, ERM/KMS, Brussels, Report 87.
DESCAMPS P. (1988) D.Sc. Dissertation, Université de l'Etat à Mons.
DESCAMPS P. *et al.* (1989) Proc. 16th Eur. Conf. on Contr. Fusion and Plasma Physics, Venice, Eur. Conf. Abstracts, Vol. 13B, Part III, p. 1053.
Equipe TFR (1985) Proc. 12th Eur. Conf. on Controlled Fusion and Plasma Physics, Budapest, Eur. Conf. Abstracts, Vol. 9F, Part II, p. 108.
GOEBEL D. *et al.* (1988) Invited paper at 8th Int. Conf. on Plasma Surface Interaction in Contr. Nucl. Fus. Devices, Jülich. *J. Nucl. Mat.* **162–164** (In press).
KOCH R. *et al.* (1986*a*) Proc. 13th Eur. Conf. on Controlled Fusion and Plasma Heating, Schliersee, Eur. Conf. Abstracts, Vol. 10C, Part II, p. 121.
KOCH R. *et al.* (1986*b*) *Computer Phys. Commun.* **40**, 1.
KOCH R. *et al.* (1987) Proc. 14th Eur. Conf. on Controlled Fusion and Plasma Heating, Madrid, Eur. Conf. Abstracts, Vol. 11D, Part III, p. 924.
KOCH R. *et al.* (1988*a*) Invited paper at the 15th Eur. Conf. on Controlled Fusion and Plasma Heating, Dubrovnik. *Plasma Phys. Contr. Fusion.* **30**, 1559.
KOCH R. *et al.* (1988*b*) Laboratory for Plasma Physics ERM/KMS, Brussels, Report 87.
LIE Y. T. *et al.* (1984) *Proc. Int. Conf. on Plasma Physics*, Lausanne, Vol. II, p. 320.
MESSIAEN A. M. *et al.* (1982) Proc. 3rd Joint Varenna-Grenoble Int. Symposium, Grenoble, Vol. 1, p. 243.
MESSIAEN A. M. and WEYNANTS R. R. (1982) *Ibid.*, Vol. 3, p. 1107.
MESSIAEN A. M. *et al.* (1984) Proc. 4th Int. Symposium on Heating in Toroidal Plasmas, Rome, Vol. 1, p. 303.
MESSIAEN A. M. *et al.* (1986*a*) *Plasma Phys. Contr. Fusion* **28**, 71.
MESSIAEN A. M. *et al.* (1986*b*) Proc. 13th Eur. Conf. on Controlled Fusion and Plasma Heating, Schliersee, Eur. Conf. Abstracts, Vol. 10C, Part II, p. 125.
POSPIESZCZYK A. *et al.* (1988) Proc. 8th Int. Conf. on Plasma Surface Interaction in Contr. Nucl. Fusion Devices. *J. Nuc. Mat.* **162–164** (In press).
SAMM U. (1983) Proc. 11th Eur. Conf. on Contr. Fusion and Plasma Physics, Aachen, Eur. Conf. Abstracts, Vol. 7D, Part II, 413.
SAMM U. and WEYNANTS R. R. (1989) Proc. 16th Eur. Conf. on Contr. Fusion and Plasma Physics, Venice, Eur. Conf. Abstracts, Vol. 13B, Part I, p. 151.
SÖLL M. and NOTERDAEME J.-M. (1985) Proc. 12th Eur. Conf. on Contr. Fusion and Plasma Physics, Budapest, Eur. Conf. Abstracts, Vol. 9F, Part II, p. 100.
TAMAI H. *et al.* (1986) *Nucl. Fusion* **26**, 365.
VANDENPLAS P. E. *et al.* (1986) Proc. 11th Int. Conf. on Plasma Physics and Controlled Nuclear Fusion Research, Kyoto, Vol. 1, p. 485.
VANDENPLAS P. E. (1987) Proc. of the Invited Papers of the 1987 Int. Conf. on Plasma Physics, Kiev, Vol. 2, p. 1162.
VAN OOST G. *et al.* (1987) *Fusion Technol.* **12**, 449.
WAELBROECK F. *et al.* (1988*a*) *Plasma Phys. Contr. Fusion*, in press.
WAELBROECK F. *et al.* (1988*b*) Proc. 12th Int. Conf. on Plasma Physics and Controlled Nuclear Fusion Research, Nice, IAEA-CN-50/A-6-1. To be published.
WAIDMANN G. *et al.* (1984) Proc. 10th Int. Conf. on Plasma Physics and Controlled Nuclear Fusion Research, London, Vol. 1, p. 193.
WEYNANTS R. R. *et al.* (1980) Proc. of the 2nd Joint Grenoble–Varenna International Symposium, Como, Vol. 1, p. 487.
WEYNANTS R. R. *et al.* (1985) Proceedings of the AIP Conference, Number 129, Sixth Topical Conference, Callaway Gardens, American Institute of Physics, p. 40.
WEYNANTS R. R. *et al.* (1987) Laboratory for Plasma Physics, ERM/KMS, Brussels, Report 85.
WEYNANTS R. R. *et al.* (1988*a*) Laboratory for Plasma Physics, ERM/KMS, Brussels, Report 88.
WEYNANTS R. R. *et al.* (1988*b*) Proc. 12th Int. Conf. on Plasma Physics and Controlled Nuclear Fusion Research, Nice, IAEA-CN-50/E-2-1.
WILSON J. R. *et al.* (1988) Proc. 12th Int. Conf. on Plasma Physics and Controlled Nuclear Fusion Research, Nice, IAEA-CN-50/E-4-1.
WINTER J. (1987) *J. Nucl. Mat.* **145–147**, 131.
WINTER J. *et al.* (1988) Proc. 8th Int. Conf. on Plasma Surface Interaction in Contr. Nucl. Fusion Devices, Jülich. *J. Nucl. Mat.* **162–164** (In press).
WOLF G. H. *et al.* (1986) *Plasma Phys. Contr. Fusion* **28**, 1413.